International Journal of GEOMATE, Feb., 2017, Vol. 12, Issue 30, pp. 160-174
Special Issue on Science, Engineering & Environment, ISSN:2186-2990, Japan
DOI: http://dx.doi.org/10.21660/2017.30.69942

SOURCE CHARACTERIZATION AND GROUND MOTION MODELING COMPUTED FROM THE 3 SEPTEMBER 2015 EARTHQUAKE, WESTERN DESERT, EGYPT

*Abd el-aziz Khairy Abd el-aal[1], Elhamy Tarabees[2] and Hazem Badreldin[1]

[1] National Research Institute of Astronomy and Geophysics, Helwan, Cairo, Egypt

[2] Geology Department, Faculty of Science, Damanhour University, Egypt

*Corresponding Author, Received: 3 Dec 2016, Revised: 14 Dec 2016, Accepted: 18 Jan 2017

ABSTRACT: To obtain the characterized source model for prediction of strong ground motions, the ground motion generation area and rupture geometry of an inland crustal earthquake from near-source ground motion records has been estimated. An earthquake, with a magnitude of 4.3 ML and a focal depth of 18 km occurred on September 3, 2015 at 30.45N, 28.44E in the Western Desert of Egypt about 60 km south of El-Dabaa city. This earthquake is the first instrumentally recorded earthquake occurring in this area in several decades. The waveform data of this event has been used for source characterization and ground motion modeling. The present work describes the results of a preliminary study conducted to obtain fault plane solutions of this earthquake from waveform inversion and P-wave polarity. For this purpose, the source parameters related to the strong ground motion were estimated by waveform data and first arrivals recorded by the Egyptian National Seismic Network (ENSN) are used to arrive at focal mechanism solutions. Fault plane solutions for the main shock indicate strike-slip motion. One nodal plate strikes about 330°, is nearly vertical, and indicates right lateral slip. The other nodal plane strikes about 240°, dips very steeply NW, and indicates left lateral slip. Also the peak ground acceleration (PGA) at the El-Dabaa site has been simulated by taking into account an accurate estimation of the source characterization, the path attenuation model, and site amplification. The results have been validated using an actual recording of PGA at one ENSN station that recorded strong ground motion.

Key words: ground motion; waveform inversion; El-Dabaa nuclear power plant site; Egyptian National Seismic Network

1. INTRODUCTION AND REGIONAL GEOLOGY

Egypt is distinguished by low to moderate earthquake activity related to the relative motions among the African, Arabian and Eurasian plates [1-4]. The divergent portion of the plate boundary between the African and the Arabian plates lies in the NNW/SSE-trending Red Sea, and connects at the northwest end to the Aqaba-Dead Sea Transform Fault and the Gulf of Suez shear zone. The Red Sea region is characterized by low to moderate shallow seismicity that lies mostly along the plate boundary or plate margins [5, 6]. Earthquakes and active volcanism within the axial trough indicate present-day rifting [5]. Low to moderate seismicity occurs in the Gulf of Suez and its extension, Fig. 1, but is scattered and has no distinct trend. Three active zones can be delineated, however. At the mouth of the Gulf, most of the activity is concentrated near the Sinai Triple Junction between Africa, Arabia, and Sinai. In the central and the northern parts of the Gulf, including the adjacent area as far as the Nile, activity decreases markedly from south to north. There is no seismological evidence that seismic activity of the Suez Rift continues into the eastern Mediterranean [1-4] and [7] as originally suggested by [8, 9]. Intra-plate seismicity occurs in Egypt west of the plate boundary and Gulf of Suez zone (e.g. Dahshour, southeast Beni-Suef and Cairo-Suez district) [7].

Intraplate seismic activity in Egypt is important because it expands the region of possible seismic hazard beyond areas immediately associated with plate boundaries. The cause of intraplate seismicity is poorly understood, and study of source mechanisms and depths of small-to-moderate size intraplate earthquakes is important to understanding the nature and origin of intraplate earthquakes.

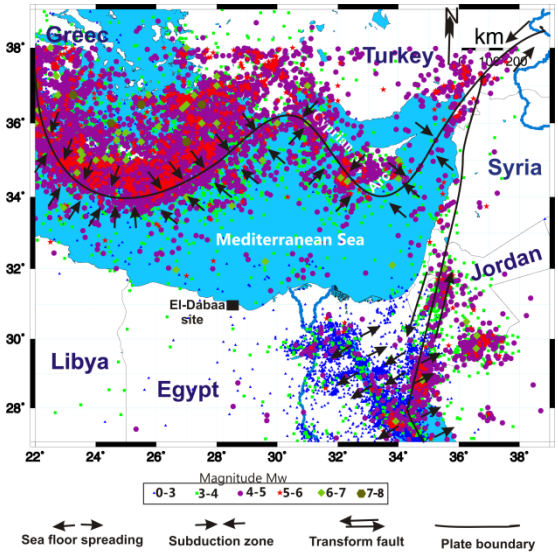

Fig.1 The figure shows main tectonic boundaries of the Eastern Mediterranean region. The earthquake data used in this map includes an update earthquake catalogue compiles from many sources, Egyptian National Seismological Network bulletins (www.nriag.sci.eg), International Seismological Center Bulletin (ISC) (http://www.isc.ac.uk/), European Mediterranean Seismological center (EMSC) (http://www.emsc-csem.org), Preliminary Determination of Epicenters, online bulletin provided by the National Earthquake Information Center (NEIC) (http://earthquake.usgs.gov/earthquakes/).

An earthquake with magnitude 4.3 ML and focal depth 18 km took place on September 3, 2015 at 30.45N, 28.44E in the Western Desert of Egypt, about 60 km south of the El-Dabaa nuclear power plant site, Fig. 2. The Mw 4.2 mainshock was felt throughout north Egypt, including the greater Cairo region, and was not followed by any significant aftershocks. The region of this earthquake has historically had very low seismicity. To understand the tectonic setting of north western Desert near the epicenter of September 3, 2015 earthquake, an accurate focal mechanism of this earthquake relocated and estimated using both P-wave first polarity and a moment tensor inversion technique applied to near-source data recorded by the ENSN local seismic network. Also, the waveform data of this event has been analyzed in detail to obtain seismic moment and fault geometry, fault area, rise time, and related source parameters to investigate the characteristics of the rupture process of the event. Finally, the peak ground acceleration (PGA) at the El-Dabaa nuclear power plant site has been simulated based on recorded ground motion by ENSN. These results plus the observed and simulated ground motions have been used to interpret the seismotectonic setting around El-Dabaa nuclear power plant site.

Two faults are reported in the area around El-Dabaa, Fig. 2. One strikes NW-SE and is revealed in geophysical studies east of Ras El Hekma [10]. The second fault also strikes NW-SE and is documented through field observations east of the Ras Abu Girab–Abu Samra monocline. The downthrown side of this fault is to the north, with displacement ranging from 8 to12 m.

Beside the above mentioned surface structures, the following major structures are known:

The El-Dabaa area is underlain by Miocene strata that dip north at 10-20° and are unconformably overlain by Pleistocene oolitic limestones. Two sets of joints occur in the Miocene lithologies, one striking EW and the second striking to the north. Pleistocene lithologies do not contain these joint sets, which brackets the timing of joint formation in the Miocene strata between the Middle Miocene and Pleistocene.

Two synclinal basins, doubly plunging synclines, are known in the El-Dabaa area; Fuka syncline and Qutaf syncline. The Fuka doubly-plunging syncline lies between the Sira monocline to the west and Ras Abu Girab-Abu Samra monocline to the east. It is occupied by alternating beds of Middle Miocene limestone and clay [11]. According to [12], the monoclines are occupied by Pliocene limestone. The Qutaf syncline lies between the eastern edge of Ras Abu Girab-Abu Samra monocline and the Sira monocline and has the same orientation as the Fuka syncline.

2. SEISMOTECTONIC SETTING AND RECENT SEISMICITY IN AND AROUND NORTHERN EGYPT

Tectonics in the Eastern Mediterranean is dominated by the relative movements of major plates (Africa, Arabia, and Eurasia) and relatively aseismic small plates East Mediterranean region, Fig. 1. The Eastern Mediterranean is a relatively small, structurally complex basin that includes a short segment of the convergent boundary between Africa and Eurasia [13]. Subduction occurs along two small arcs, the Hellenic and Cyprian arcs, Fig. 1. In both places, subduction has been documented using bathymetric, earthquake hypocentres and other relevant geophysical data. However, a study of the Mediterranean area tectonics and geodynamics can be of high interest although very complicate, because, in this zone, the convergent stress field, active for the last hundreds of millions of years, produced a number of very different tectonic systems.

The recent seismological studies [13-14] indicated that the seismicity is much higher in the area of the Hellenic arc than in the Cyprean arc, Fig. 1. Moreover, the activity occurs in a wide belt suggesting that the plate boundary is a deformation zone instead of a single line. [13-14] suggested that the present tectonics is the result of the collision of the African-Eurasian plates, the Arabian- Eurasian convergence and the lateral motion, towards the west, of the Anatolian-Aegean subplate. The boundary between Africa and Anatolian- Aegean subplate is delineated by the Hellenic arc, the Pliny Strabo trench, the Florence Rise and Cyprus in the west, whereas in the east, the boundary has been identified in the Herodotus basin or east of Cyprus [13]. The relative motion of the African plate relative to fixed Eurasia has a direction, which varies within north-west and northeast. Using recent space geodesy data, [14] confirm this overall trend, in which, relative to Eurasia, Africa has a north– south component of convergence of about 6 ± 2 mm year^{-1} , Anatolia moves westward with a velocity of 24 ± 2 mm year^{-1} and the south-western Aegean Peloponnesus towards SSW at 30 ± 2 mm year^{-1}. Although most authors agree about the existence of a wide ocean separating Africa and Eurasia (Palaeotethys) at least by late Palaeozoic time, there is a little agreement about how, when and where this ocean formed and was ultimately consumed [15].

The recent seismological studies indicated that the Hellenic arc is generated by the active subduction of the oceanic lithosphere in the east Mediterranean with a NE-SW direction, Fig. 1. It is a very small and bent arc with a slab subducting at a low angle (about 30°), as indicated by the geometry of the Benioff Zone.

We stated from the focal mechanisms of recent earthquakes it is easy to infer the complexity of the Hellenic arc system. The present seismicity is the more intense of the whole Mediterranean basin for all the magnitude intervals. The few magnitude events equal or greater than 6 are almost all concentrated at the northern termination of the trench. From recent seismicity map, it is easy to notice that the Greek coast and western Turkey are, along with the Hellenic Arc, are the most active seismic areas of the Mediterranean basin and of the whole Alpine-Himalayan chain. Here the largest number of earthquakes with magnitude greater than 6 appear to occur. The prevalently extensive and trans current tectonics of the northern and central Aegean is controlled by the westward movement of Turkey and by southeastward movement of the Hellenic arc, both with respect to the Euro- Eurasia plate [13-14].

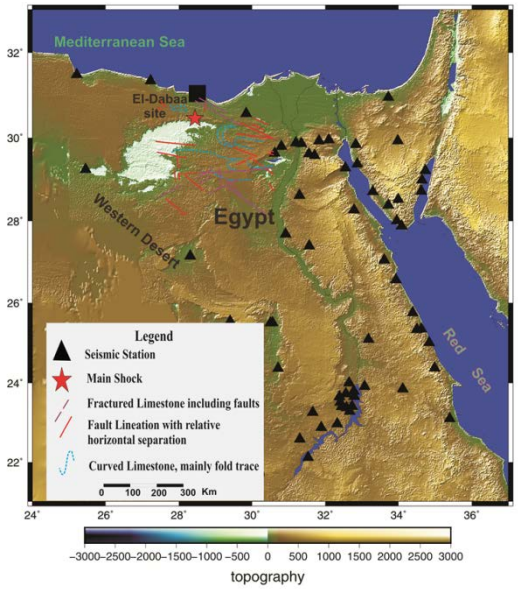

Fig.2 Epicenteral location map of September 3, 2015 earthquake (red star) and the Egyptian national seismological network (black triangle) which includes both very broadband and broadband and short period. The black square in map is El-Dabaa nuclear power plant site. The structural elements around El Dabaa area are shown according to, [16].

3. EARTHQUAKE DATA ANALYSIS

3.1. Waveform Inversion And Earthquake Source Characterization

In this study, we have found that so far, polarity data alone were insufficient to constrain a well-controlled fault-plane solution. Therefore, waveform modeling is the only way to achieve significant improvements in the source mechanism solution. Therefore, to understand the type of slip of September 3 2015 earthquake, we estimated an accurate focal mechanism of this event using a moment tensor inversion technique of near-source data recorded by the Egyptian National Seismic Network (ENSN). ENSN has 66 seismic stations (10 very broadband stations, 16 broadband stations, one borehole station, 40 short period stations) distributed in and around Egypt, plus one main acquisition center at Helwan City and five sub-centers at Burg El-Arab, Hurghada, Mersa Alam, Aswan and Kharga City, Fig. 2. The main centre receives seismic data from the near distance stations through telemetry communications and from some of the more distant stations via satellite communications. The sub-centers collect data from the nearest stations and also send it to Helwan via satellite. More details about ENSN sensors, acquisitions, and data processing and analysis can be found in [17-18].The dramatic increase in

deployment of broadband and very broadband seismic stations in Egypt after 2009 with real-time continuous telemetry has meant that moment tensor determinations have become increasingly feasible, and moment tensor solutions are now a very important product of ENSN.

We used a very well-established method [19-22] and software to perform waveform inversion for the main shock of the 3 September, 2015 earthquake south of El-Dabaa city using waveform data recorded by ENSN broadband and very broadband stations, Fig. 3. This method provides a reliable way to estimate the moment tensor solutions for small and moderate earthquakes, isolating the propagation term and eliminating the effects of site amplification.

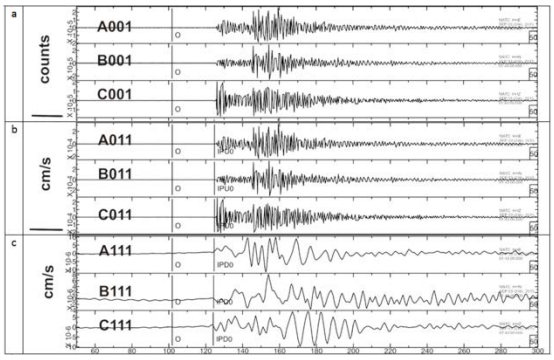

Fig.3 The processing steps applied at waveform data of September 3, 2015 recorded at seismic station named SWA from ENSN. From the top to the bottom as fellows: a , panels A001, B001 and C001 are the raw waveform of EW, NS and vertical component (Counts/(m.s^{-1}); b, panels A011, B011 and C011 are velocity waveform of EW, NS and vertical component after picking and deconvolved with instrumental response; and c, panels A111, B111 and C111 are velocity waveform of EW, NS and vertical component after low pass filtering.

In the common form, the displacement $\boldsymbol{d}$ at (c) station's component at position (x) at time (t) can then be calculated from the convolution of the Green's function $\boldsymbol{G}$ and the moment tensor $\boldsymbol{M}$.

$$\boldsymbol{d_c(x,t)} = \sum_{q=1}^{6} \iiint_{v} \boldsymbol{G_{xcq}(t,\xi) * M_q(t,\xi) d\xi + e_{xc}(t)} \qquad (1)$$

where *e* is the observed error. The volume change during an earthquake is too small to be detected, therefore we can neglect the volume change component $\boldsymbol{M_6}$. We also can assume a simple point source model in which the seismic waveform radiated from one point, allowing us to rewrite equation 1 as re-written:

$$\boldsymbol{d_c(x,t)} = \sum_{q=1}^{5} \boldsymbol{G_{xcq}(t,\xi_c) * M_q(t) + e_{xc}(t)} \qquad (2)$$

where $\boldsymbol{\xi_c}$ is the location of the centroid. Because the focal mechanism is kept constant during the earthquake, we approximated the shape of the source time function to be an isosceles triangle with a half duration of $\boldsymbol{t_r}$, allowing us to rewrite equation 2 as follows:

$$\boldsymbol{d_c(x,t)} = \sum_{q=1}^{5} \boldsymbol{G_{xcq}(t,t_r,\xi_c) \times M_q(t) + e_{xc}(t)} \qquad (3)$$

After applying a low-pass filter to the observed data, an N–dimensional data matrix is obtained. The solution of the matrix equation is obtained by the least squares approach. [22] assumed that the horizontal location of the centroid can be approximated as the epicentre of an earthquake, and they demonstrate how it is possible to estimate the optimal depth of the earthquake using the grid-search method. For more details about the waveform inversion technique and new software, please refer to [19 and 20] and [22 and 23].

We performed an inversion technique, where we processed and analyzed the waveform data of the mainshock and removed the instrument response during the processing steps by deconvolution of response file for each seismometer. For all earthquake data, we used 100–200 sec waves and a frequency range of 0.01–0.1. Then, the data have been down sampled with a 1-Hz rate.

We used the crustal structure of [24 and 25] as shown in Fig. 4. These crustal models give the smallest arrival time residuals and low uncertainty in latitude and longitude among all the crustal models proposed for Egypt and its vicinity. Fig. 5a illustrates the observed and synthetic waveform and the corresponding moment tensor solution for the mainshock. The obtained moment tensor solution indicates strike slip faulting with a minor oblique component, Fig. 5a.

3.2. Focal Mechanism Determined From First Polarity

The source of a small earthquake is typically approximated by a double-couple point source, or focal mechanism, derived from observed P-wave first-motion polarities. A focal mechanism divides a reference sphere around the source into four quadrants, two in which the first motions are away from the source, and two in which first motions are toward the source.

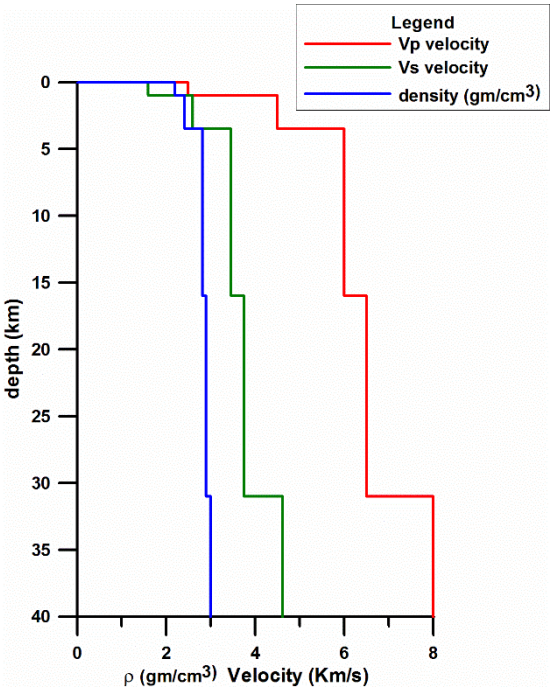

Fig.4 P-wave, S-wave velocity and density model for northwestern region in Egypt [24 and 25].

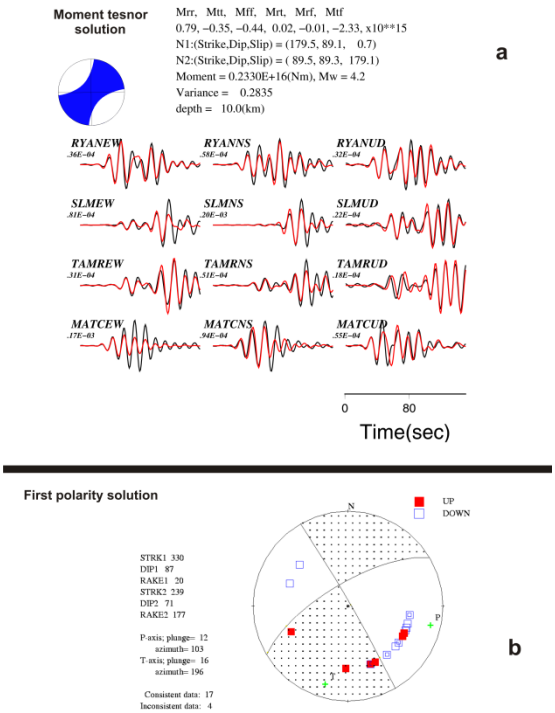

Fig.5 Panel (a) of the figure shows moment tensor solution and waveform fits for moment tensor inversion of September 3, 2015 earthquake. The black lines are the velocity data, and the red lines are the synthetics. Both are in cm and filtered using the same pass band. Panel (b) of the figure illustrates focal mechanism of the same event as obtained using P-wave first polarity.

First-motion polarities are observed at seismic stations, and the position on the focal sphere for each observation is determined by the azimuth and takeoff angle at which the ray leaves the source, based on an assumed location and seismic-velocity model. A focal mechanism is then found that best fits the first-motion observations. Fig. 5b shows the focal mechanism for the main shock determined from P-wave first polarity.

3.3. Source Parameters

The study of earthquake source parameters and faulting processes of small earthquakes is important for clarifying the scaling of earthquake sizes and stress drops. Although kinematic earthquake-source models are not satisfactory in terms of rupture dynamics, they provide reliable results in terms of stress drop and coseismic slip distribution. To calculate the source parameters of this earthquake, we wrote a MATLAB code to calculate the average spectrum and then estimate source parameters. The records of the vertical component for every station were corrected to a zero baseline and instrument response. We selected 8-second P-wave signal windows to avoid contamination from other phases and maintain the resolution and stability of the spectra.

We inverted the average spectrum using the simplified functional form of the source spectrum with a single corner frequency, as described by the [26, 27] equation:

$$S(f) = \Omega_o / [1 + (f / f_c)^{2\gamma}]^{1/2} \quad (4)$$

In equation (4), the spectral parameters Ω_o, f_c and γ represent the low-frequency amplitude level, the corner frequency, and the high-frequency spectral fall-off above the corner frequency, respectively. By assuming Brume's model ($\gamma = 2$) and using the [28] relations, we obtained:

$$r_o = \frac{2.34(V_p)}{2\pi f_o} \quad (5)$$

$$\Delta\sigma = \frac{7M_o}{16(r_o)^3} \quad (6)$$

where V_p is the P-wave velocity, f_o is the corner frequency and M_o is the seismic moment. The total ruptured area that can be calculated by the relation of [29] is:

$$A = \pi(V_r t / 2)^2 \quad (7)$$

where V_r is the rupture velocity (typically V_r is in the range 0.7- 0.9V_s, being V_s the shear wave velocity), while *t* represents the rupture duration. The term $V_r t/2$ represents the fault radius (r_o). The calculated source parameters of the earthquake are listed in Table (1).

Table 1 Earthquake source parameters

no	Date (d/m/y)	Time (h:m)	$\Delta\sigma$ (bar)	r_0 (km)	Rupture Area (km^2)	Dislocation (m)
1	3/9/2015	01:44	142.6	0.41	0.54	0.1212

3.4. Synthetic Earthquake Simulation And Peak Ground Acceleration Modeling

Predicting strong ground motion is essential to estimating the potential hazard from future earthquakes. Because there are no ground motion records from the area of the El-Dabaa nuclear power plant site for the September 3, 2015 earthquake, we calculated a synthetic ground motion model. The seismological model of [30] is well-suited for generation of synthetic acceleration-time response [31]. We developed a synthetic ground motion and spectral acceleration at rock level at the El-Dabaa nuclear power plant site by considering calculated magnitude and hypocentral distance from the mainshock. Stochastic modeling of high frequency shear wave ground motion [32] is a simple and powerful technique for calculating ground motions and is mainly based on the hypothesis that the predicted ground motion at a site can be simulated in a deterministic way, with a random phase spectrum modified, such that the predicted motion is distributed over a time interval related to magnitude of the specified earthquake and distance from source. This method is known as the stochastic method, where the energy is distributed randomly over the duration of the source. The contributions from the earthquake source (E), path (P), site (G) are modeled to obtain the total spectrum of the motion at a specific site. For more comprehensive summary about the method, refer to the work of [1, 2] and [30]. In the current work, the PGA predicted from mainshock of the 3 September, 2015 earthquake is calculated.

One important step of our analysis includes the validation of the stochastic model parameters at the free-field station that recorded the earthquake. We compared recorded PGA and simulated PGA computed with the used stochastic method for mainshock of the 3 September, 2015 earthquake. This event was recorded by some strong ground motion stations. We simulated the event at location of the station, namely ANS station where a strong motion instrument exist, taking into consideration the local site condition of the station. The station was located at coordinates 30.29N and 31.40E northeast of Cairo city. The recorded and simulated PGAs at that station resulting from this earthquake were 0.55 gal and 0.52 gal, respectively. Comparisons are made for horizontal-component peak ground accelerations. The observed motions are in reasonable agreement with the simulated. It was found a big similarity between simulated and recorded values. Indeed, the local match between synthetic computations and the few observations available for of September 3, 2015 earthquake encourages the extension of the applicability of our calculations at El-Dabaa nuclear power plant site which felt this earthquake, where no surveys or observations are available, Figs. 6, 7.

4. DISCUSSION CONCLUSION

This work describes the results of a study conducted to obtain fault plane solutions of an earthquake occurring on September 3, 2015from waveform inversion and P-wave polarity. This earthquake occurred in a region of relatively low seismicity where earthquakes above the magnitude threshold of the Harvard CMT catalog have been not recorded. We used waveform data and first arrivals recorded by ENSN to determine focal mechanism solutions.

We estimated the focal mechanism of this earthquake using both P-wave first polarity and a moment tensor inversion technique applied to near-source data recorded by the ENSN local seismic network. We analyzed the waveform data of this event in detail to obtain seismic moment and fault geometry, fault area, rise time, related source parameters to investigate the characteristics of the rupture process of the respective event.

The constructed fault plane solutions for the mainshock indicate strike slip faulting. One nodal plate strikes about 330°, is nearly vertical, and indicates right lateral slip. The other nodal plane strikes about 240°, dips very steeply NW, and indicates left lateral slip. The obtained result is that NW-SE-oriented nodal planes are in good agreement with both surface and subsurface faults affecting the epicenteral region Moreover, the source characterization and ground motion modeling are obtained to understand the tectonic setting around El-Dabaa nuclear power plant site. This earthquake has been analyzed and used for simulating the PGA at Dabaa nuclear power plant site.

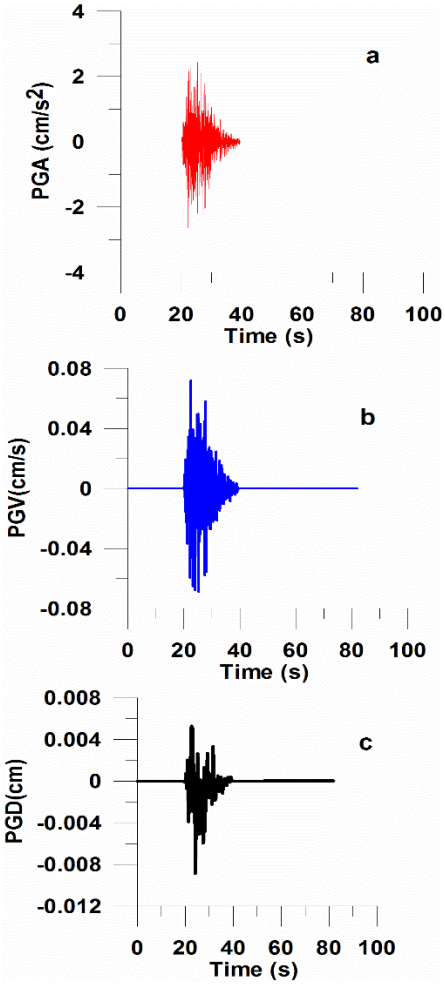

Fig.6 The simulated time history) of September 3, 2015 earthquake including peak ground acceleration (PGA) at (panel a), peak ground velocity (PGV) at (panel b) and peak ground displacement (PGD) at (panel c) at El-Dabaa nuclear power plant site.

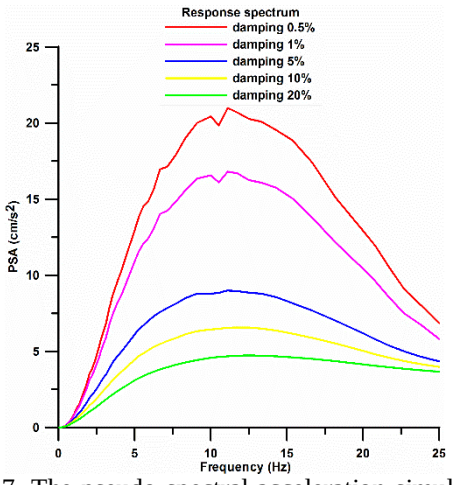

Fig. 7. The pseudo spectral acceleration simulated from September 3, 2015 earthquake with 0.5%, 1%, 5%, 10% and 20% damping at El-Dabaa nuclear power plant site.

5. CONCLUSION

Our waveform analysis for the September 3, 2015 earthquake indicates:

1- The seismic moment is 0.2330 x10^{16} Nm, equivalent to Mw 4.2.
2- The focal depth determined by waveform inversion technique is 10 km.
3- The fault plane solution is highly consistent with the surface and subsurface faults affecting the region.
4- The moment tensor and first polarity techniques yield faulting mechanism with strikes of 179.5° and 330°, dips of 89° and 87°, rakes of 0.7° and 20°, respectively.
5- We found little difference in fault pane solution obtained by both techniques for this earthquake, and we interpret differences between the two solutions to be due to lack of azimuthal station coverage and lack of knowledge of precise crustal structure. The best-fitting focal mechanism depends on P-wave polarity observations, earthquake location, and velocity model. The stability of a focal mechanism solution is most sensitive to changes in the vertical velocity gradient. The calculated source parameters of this event indicate that the rupture area is approximately 0.54 km^2, fault radius is 0.41 km, stress drop is 142 bar and a dislocation is 0.12 m.

Because there are no strong motion stations near the nuclear power plant site at that time, we simulated PGA from this earthquake at El-Dabaa nuclear power plant site using ground motion recorded by the ENSN. We used both the obtained results and the observed and simulated ground motions for seismotectonic setting interpretations. We concluded that the background seismicity suggests that the level of seismicity is typically low in the Western Desert of Egypt. Reviewing the historical period and the instrumental monitoring began only two or three small to moderate events were reported.

6. ACKNOWLEDGMENT

The authors thank the Egyptian National Seismic Network, which provided us with digital real seismic data. Figures were generated by SAC, the Generic Mapping Tools (GMT), and Golden software (Grapher). Grateful thanks to Barbara Tewksbury (Department of Geosciences, Hamilton College, NY, USA) who helped improve and edit the manuscript. The author appreciates comments

and revisions from the reviewers, which improved the manuscript. The authors are also grateful to editor of Geodinamica Acta who gave us a chance to improve the manuscript.

7. REFERENCES

[1] Abd el-aal A. K. (2008). Simulating Time-Histories and Pseudo-Spectral Accelerations from the 1992 Cairo Earthquake at the Proposed El-Fayoum New City Site, Egypt Acta Geophysica 56:1025-1042, doi: 10.2478/s11600-008-0054-6.

[2] Abd el-aal A. K. (2010a). Modeling of seismic hazard at the northeastern part of greater Cairo metropolitan area, Egypt. J. Geophys. Eng. 7, 75–90, doi:10.1088/1742-2132/7/1/007, 2010.

[3] Abd el-aal A. K. (2010b). Ground motion prediction from nearest seismogenic zones in and around Greater Cairo Area, Egypt. Nat Hazards Earth Syst Sci 10:1495–1511, doi: 10.5194/nhess-10-1495-2010.

[4] Badawy, A., 1996. Seismicity and kinematic evolution of the Sinai plate. Ph D thesis, pp115, L. Eötvös Univ. Budapest.

[5] Fairhead, J.D, and Girdler, R.W. (1970). The seismicity of the Red Sea, Gulf of Aden and Afar Tiangle, Phil. Trans. Roy. Soc. London A 267, 49-74.

[6] Makris J. and Henke C.H. (1992). Pull-apar evolution of the Red Sea, J. Petrol. Geol. 15, 2, 127-134. Moores, E.M., and R.J. Twiss, 1995, Tectonics, W.H. Freeman and Co., New York, 415 pp.

[7] Abou Elenean K.M. (2007). Focal mechanisms of small and moderate size earthquakes recorded by the Egyptian National Seismic Network (ENSN), Egypt. NRIAG J. Geophys. 6, 117–151.

[8] Kebeasy R., Maamoun M., and Albert R. (1981). Earthquake activity and earthquake risk around the Alexandria area in Egypt. Acta Geophysica Polonica 29(1):37–48.

[9] Kebeasy R. (1990). "Seismicity" in Geology of Egypt (R. Said, Ed.) A.A. Balkerma, Rotterdam, 1990, 51-59.

[10] Hammad, F. A. (1972). The geology of soil and water resources in the area between Ras E l Hekma and Ras Alam El Rum, Western Mediterranean Littoral Z one, Egypt. Ph.D. Thesis, Fac. Sc., Cairo Univ.

[11] Paver, G. L. and Pretorious. (1954). Report on the reconnaissance hydrogeological investigation in the Western Desert Coastal Zone. Publ. Inst. Desert, Egypt, No5, 145 p.

[12] El Shamy, I. Z. (1968). The geology of water and soil resources in El Dabaa area Western Mediterranean coastal zone U.A.R. M.Sc. Thesis, Fac. Sci, Cairo Univ.

[13] Ali E. Aksu, , Jeremy Hall and Cenk Yalt Vrak, 2005.Miocene to Recent tectonic evolution of the eastern Mediterranean: New pieces of the old Mediterranean puzzle, Marine Geology 221 (2005) 1–13

[14] McClusky, S., Balassanian, S., Barka, A., Demir, C., Ergintav, S., Georgiev, I., Gurkan, O., Hamburger, M., Hurst, K., Kahle, H., Kastens, K., Kekelidze, G., King, R., Kotzev, V., Lenk, O., Mahmoud, S., Mishin, A., Nadariya, M., Ouzounis, A., Paradissis, D., Peter, Y., Prilepin, M., Reilinger, R., Sanli, I., Seeger, H., Tealeb, A., Toksöz, M.N. and Veis, G. (2000). Global Positioning System constraints on plate kinematics and dynamics in the eastern Mediterranean and Caucasus. Journal of Geophysical Research 105: doi: 10.1029/1999JB900351. issn: 0148-0227

[15] Robertson A. H. F. and Mountrakis D. (eds) (2006). Tectonic Development of the Eastern Mediterranean Region. Geological Society Special Publication no. 260. vi + 717 pp. London, Bath: Geological Society of London.

[16] Allam, A, El-Khashab, H, Maamoun, M, and Ibrahim E.(1979). Studies on seismicity in the area of El-Dabaa, Zaafrana and south Safaga nuclear power planet sites. Bull. Helwan Inst. Geophysics. Pp 1-98

[17] Abd el-aal A. K. (2013). Very broadband seismic background noise analysis of permanent good vaulted seismic stations. J Seismol 17:223–237. doi: 10.1007/s10950-012-9308-5.

[18] Abd el-aal A. K., Soliman M. S. (2013). New seismic noise models obtained using very broadband stations. Pure Appl Geophys 170: 1849–1857. doi: 10.1007/s00024-013-0640-7.

[19] Abd el-aal A. K., Yagi Y., Abdelrahman K. (2016a). Earthquake source characterization, moment tensor solutions, and stress field of small - moderate earthquakes occurred in the Northern Red Sea Triple Junction. Geosciences journal, accepted.

[20] Abd el-aal A. K., Yagi Y., Kamal H., Abdelrahman K. (2016b). Implementation of integrated multi-channel analysis of surface waves and waveform inversion techniques for seismic hazard estimation. Arab J. Geosci., 9:322, doi: 10.1007/s12517-016-2329-6.

[21] Abd el-aal A. K., Badreldin H. (2016). Seismological aspects of the 27 June 2015 Gulf of Aqaba earthquake and its sequence of aftershocks. J Seismol. doi: 10.1007/s10950-016-9572-x.

[22] Yagi Y. and Nishimura N. (2011). Moment tensor inversion of near source seismograms. Bulletin of IISEE, 45, 133–138.

[23] Yagi Y and Fukahata Y (2012). Introduction of uncertainty of Green's function into waveform inversion for seismic source processes. Geophysical Journal International 186 (2): 711-720.

[24] Makris J., Stoefen B., Vees R., Allam A., Maamoun M. and Shehata W. (1979). Deep seismic sounding in Egypt, Part I Unpublished technical report, Inst. für Geophys. Univ. Hamburg, Hamburg, 20 pp.

[25] El Hadidy S. (1995). Crustal structure and its related causative tectonics in Northern Egypt using geophysical data, Ph.D. Thesis, Ain Shams University Cairo, Egypt.

[26] Boatwright J. (1978). Detailed spectral analysis of two small New York state earthquakes. Bull. Seismol. Soc. Am. 69, 49–79.

[27] Boatwright J. (1980). A spectral theory for circular seismic sources: simple estimates of source dimension, dynamic stress drop and radiated energy. Bull. Seism. Soc. Am. 70, 1–27.

[28] Hanks, T. C. and 11. Wyss, The use of body-wave spectra in the determ1nation of seismic source parameters, Bull. Seismo1. Soc. Amer., 62, 1n press, 1972

[29] Fukao Y. and Kikuchi M. (1987). Source retrieval for mantel earthquakes by iterative deconvolution of long-period P-wave. Tectonophysics 144 249-269.

[30] Boore, D. M. (1983). Stochastic simulation of high frequency ground motions based on seismological models of the radiated spectra. Bull. Seism. Soc. Am., 73, 1865-1894, 1983.

[31] Atkinson G. M., and Boore, D. M. (1995). Ground motion relations for eastern North America. Bull. Seism. Soc. Am. 85, 17-30, 1995.

[32] Boore, D. M. (2003). Simulation of ground motion using the stochastic method. Pure Appl. Geophy. 160, 635–676.